Scaling laws of velocity gradient moments of attached eddies

X. X. Li,[1] R. F. Hu,[2,*] and L. Fang[1,3,†]

[1]*Laboratory of Complex Systems, Ecole Centrale de Pékin, Beihang University, Beijing 100191, China*

[2]*Center for Particle-Laden Turbulence, Key Laboratory of Mechanics on Disaster and Environment in Western China, Ministry of Education, and College of Civil Engineering and Mechanics, Lanzhou University, Lanzhou, Gansu, China*

[3]*Research Institute of Aero-Engine, Beihang University, Beijing 100191, China*

(Received 21 February 2024; accepted 16 August 2024; published 3 September 2024)

Townsend's attached-eddy model (AEM) is one of the most widely used models in explaining and predicting the logarithmic region of wall turbulence. Townsend pioneered the postulate that wall-attached eddies exhibit self-similar velocity distributions. This premise has led to the derivation of velocity variance scalings in the logarithmic region. In particular, the attached eddies have been extracted at moderate scales and have been illustrated to contain the most kinetic energies in the logarithmic region. In the present contribution, we derive analytically the scalings of the moments of velocity gradients of attached eddies by using the AEM. The direct numerical simulation data with the moderate-scale extraction of attached eddies show good agreement with the derived scalings. Moreover, the contributions of different-scale structures to the moments of velocity gradients are compared, showing that the wall scalings of all-scale velocity gradients are interestingly half of moderate-scale attached eddies. This also indicates the non-negligible influence of the small-scale eddies on the velocity gradients in the logarithmic region. In addition, there are departures in the moments of velocity Hessian, inspiring future improvement in the extraction method of attached eddies.

DOI: 10.1103/PhysRevFluids.9.094602

I. INTRODUCTION

Turbulence has been dubbed the "problem of the century" since it is widely considered to be one of the most challenging problems in classical physics. The development of a feasible physical model for wall turbulence is known to be a challenging task due to its intrinsic complexity. Specifically, the logarithmic region of wall turbulence has attracted a lot of interest [1,2] due to its significance in turbulence momentum and kinetic energy generation and transfer, for which the attached-eddy model (AEM) can act as a fundamental physical model. In recent years, lots of efforts have been made to expand the AEM to explain more phenomena in wall turbulence [3–8].

Initially proposed by Townsend [3], the attached-eddy hypothesis (AEH) concentrates on the equilibrium layer. Townsend emphasized that within the equilibrium layer, viscous stress is significantly lesser compared to Reynolds stress, leading to an approximation where the wall stress is nearly equivalent to the Reynolds stress. Moreover, the equilibrium layer's nearly constant nature is suggested by the little variation in Reynolds stress within it. Consequently, it is usually also referred to as the "constant-stress equilibrium layer," which essentially corresponds to the logarithmic region of wall turbulence. The spirit of the AEH is related to the turbulence energy distribution within the

*Contact author: hurf@lzu.edu.cn

†Contact author: le.fang@buaa.edu.cn

constant-stress equilibrium layer. Townsend assumed that the sizes of the primary attached eddies in this layer are proportional to the distance from the wall [3]. In other words, the velocity fields of the energy-containing attached eddies can extend to the wall, and in a sense, they are attached to the wall. Therefore, Townsend named these eddies as "attached eddies." He further assumed that the logarithmic region can be conceptualized as a collection of a hierarchy of such eddies that share a similar velocity distribution. Additionally, the probability density function of these eddies is found to be inversely proportional to their height. This led to the determination of the velocity covariance function for a flow composed of attached eddies, as given by

$$R_{ij}(x_3) = \int_{h_{\min}}^{h_{\max}} p(h) I_{ij}(x_3/h) dh, \tag{1}$$

where $R_{ij} = \langle u_i u_j \rangle$ is the velocity covariance (the angle brackets denote ensemble average), $h_{\min}$ and $h_{\max}$ are the minimum and maximum height of attached eddies, respectively, with $h^+_{\min} \approx 100$ and $h_{\max} \sim \delta$ [4,9], x_3 is the normal distance to the wall, I_{ij} is the contribution to the correlation function from attached eddies of height h (intensity function), $p(h)$ is the probability density function of attached eddies, and δ is the thickness of the turbulent boundary layer. Following this, Townsend derived the second-order moments of velocity fluctuations as

$$\langle u_1^2 \rangle = A_1 \ln(\delta/x_3) + B_1, \tag{2}$$

$$\langle u_2^2 \rangle = A_2 \ln(\delta/x_3) + B_2, \tag{3}$$

$$\langle u_3^2 \rangle = B_3, \tag{4}$$

where u_1, u_2, and u_3 are the streamwise, spanwise, and wall-normal velocity fluctuations, respectively, and A_1, A_2, B_1, B_2, and B_3 are constants. The AEM has been widely revisited and developed in recent years, leading to a series of theoretical results which are in agreement with real turbulence. For example, Meneveau and Marusic [10] indicated that all even-order moments of streamwise velocity fluctuation behave logarithmic functions of the distance from the wall with the assumption of Gaussian velocity distribution. de Silva *et al.* [11] obtained logarithmic scalings for second- and higher-order structure functions. Yang and co-workers found several new scalings in wall turbulence [12–14]; Xie *et al.* [15] obtained the logarithmic scaling of the third-order structure function in the logarithmic region of wall turbulence. Experimental measurements and numerical simulations have provided a large amount of support for the scaling laws predicted by the AEM [2,10,16–28]. Meanwhile, many reduced-order and data-driven methodologies have demonstrated remarkable efficacy in elucidating the characteristics of attached eddies and corroborating their statistical rules [29–36].

The attached eddies have long been presumed to play an important role in momentum transfer in the logarithmic layer [3,6,29,37,38], and one can anticipate that they may also contribute to energy transfer. Indeed, several studies have investigated the interscale energy transfer in wall turbulence by spectral budget analysis [39–44]. In addition, the interscale energy transfer of turbulence can also be probed via velocity gradients. In isotropic turbulence, it has been shown that the relation between second- and third-order moments of velocity gradients can be represented by the Karman-Howarth equation [45]. Specifically, in physical space, the interscale energy transfer can be quantitatively represented by involving the concept of the third-order moments of the velocity gradients [46]. In anisotropic turbulence, the interscale energy transfer is still not well explained yet, but some recent studies imply that it might be analogical to the isotropic flows. For example, Fig. 17 of Ref. [47] shows that all components in an anisotropic flow lead to positive values of third-order moments of the velocity gradients in early transition, indicating an inverse energy transfer from small to large scales. In this sense, it may be interesting to dig a little more into the energy transfer by attached eddies. Towards this direction, the first step is then to investigate the prediction of the AEM on the moments of velocity gradients.

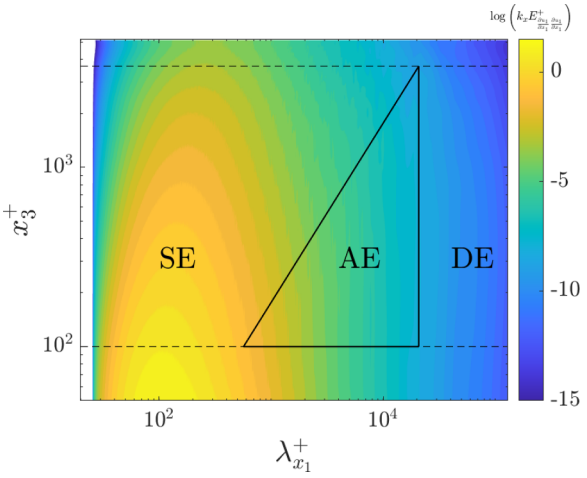

FIG. 1. Premultiplied spectrogram of the streamwise velocity gradient $\partial u_1/\partial x_1$ at $\mathrm{Re}_\tau = 5200$, where SE, AE, and DE denote small-scale eddies, attached eddies, and detached eddies, respectively, which are defined by Hu *et al.* [23].

As discussed earlier, attached eddies are assumed to contain significant energies, and they are at moderate scales [23]. However, velocity gradients are small-scale quantities. It is then natural to believe that the AEM cannot capture all-scale velocity gradients but only moderate scales. It can be seen from Fig. 1 that the small-scale eddies contain the majority of the streamwise velocity gradient. Despite this, it may be still insightful to study the moderate scales first, as they are turbulent structures associated with energy production [41]. Therefore, the present contribution aims to focus on the moderate-scale structures which can be represented as attached eddies, to show the prediction of the AEM by comparing with the direct numerical simulation (DNS) extraction, and finally to compare with all-scale energy transfer.

The structure of this paper is organized as follows. In Sec. II, we show the derivation of the moments of velocity gradients of attached eddies with arbitrary order by the AEM. Section III examines the derived scaling laws of velocity gradient moments from the DNS data of turbulent channel flows, where the contributions of different scales to the moments of velocity gradients are extracted. More results are shown in Sec. IV for the scalings of moments of higher-order velocity derivatives. Conclusions are presented in Sec. V.

II. THEORY

In this section, we will revisit the model of Woodcock and Marusic [5], which rigorously refined the original model of Townsend and meticulously derived all moments of velocity in the logarithmic region, employing a more rigorous mathematical approach for attached-eddy modeling. Then, we will extend this approach to the moments of velocity gradients.

A. Model of Woodcock and Marusic

One of the key points in the AEM is that the attached eddies have similar velocity distributions regardless of their sizes. The velocity at $\boldsymbol{x}$ is denoted as [5]

$$\boldsymbol{U}_{\text{one eddy}} = \boldsymbol{Q}\left(\frac{\boldsymbol{x}-\boldsymbol{x}_e}{h}\right), \tag{5}$$

where $\boldsymbol{x}_e$ is the center of an attached eddy, h is the height of the attached eddy, and the self-similar velocity distribution function $\boldsymbol{Q}$ can be determined from the Biot-Savart's law. According to the

AEM, all attached eddies are independent of each other, therefore the expression for the velocity induced by all attached eddies at $\boldsymbol{x}$ is

$$\boldsymbol{U}_{\text{total}} = \sum_{k=1}^{n_0} \boldsymbol{Q}\left(\frac{\boldsymbol{x}-\boldsymbol{x}_k}{h_k}\right), \tag{6}$$

where $\boldsymbol{x}_k$ is the center of the kth attached eddy, h_k is the height of the kth attached eddy, and n_0 is the number of attached eddies.

To derive an arbitrary moment of velocity in the logarithmic region by attached eddies, some useful quantities need to be defined [5]. Firstly, the probability density function of attached eddies follows a -1 power law of h as [3,4]

$$p(h) \propto \frac{1}{h}, \tag{7}$$

where $\int_{h_{\min}}^{h_{\max}} p(h)dh = 1$, hence, we have

$$p(h) = \frac{1}{\ln(h_{\max}) - \ln(h_{\min})}\frac{1}{h}. \tag{8}$$

Then, the velocity contribution function of attached eddies is defined as

$$I_{k,l,m}(X_3) \overset{\text{def}}{=} \iint_{-\infty}^{+\infty} Q_1^k(\boldsymbol{X})Q_2^l(\boldsymbol{X})Q_3^m(\boldsymbol{X})dX_1dX_2, \tag{9}$$

where $\boldsymbol{X} = (X_1, X_2, X_3) = (x_1/h, x_2/h, x_3/h)$ (x_1, x_2, and x_3 are the streamwise, spanwise, and wall-normal coordinates, respectively), and $I_{k,l,m}(X_3)$ is an integral in the X_1-X_2 plane. Another important quantity is the cumulants of velocity, defined as

$$\lambda_{k,l,m}(x_3) \overset{\text{def}}{=} n_0 \int_{h_{\min}}^{h_{\max}} I_{k,l,m}(X_3)p(h)dh. \tag{10}$$

When it comes to the mean velocity [5], we have $\langle U_1\rangle = \lambda_{1,0,0}$, $\langle U_2\rangle = \lambda_{0,1,0}$, $\langle U_3\rangle = \lambda_{0,0,1}$, which means that the cumulants of velocity are essentially equivalent to the averaging Eq. (6) in this case. Then we follow Ref. [5] to assume that an attached eddy does not contribute to the velocity field whose location is beyond the height of the eddy, i.e.,

$$\boldsymbol{Q}(\boldsymbol{X}) \approx 0, \ \text{for}\ x_3 > h. \tag{11}$$

Using this assumption, Eq. (10) becomes

$$\lambda_{k,l,m}(x_3) = \begin{cases} n_0 \int_{x_3}^{h_{\max}} I_{k,l,m}(X_3)p(h)dh, & \text{for} \quad x_3 > h_{\min}, \\ n_0 \int_{h_{\min}}^{h_{\max}} I_{k,l,m}(X_3)p(h)dh, & \text{for} \quad x_3 \leqslant h_{\min}. \end{cases} \tag{12}$$

Considering the case of logarithmic region, we have $x_3 > h_{\min}$. Substituting Eq. (8) and the Taylor series of $I_{k,l,m}(X_3)$ at $X_3 = 0$ into Eq. (12), and integrating X_3 by replacing the variable h with X_3, a concrete expression for the cumulants of velocity can be obtained as

$$\begin{aligned} \lambda_{k,l,m}(x_3) &= \beta\left[-I_{k,l,m}(0)\ln\left(\frac{x_3}{h_{\max}}\right) + \sum_{n=1}^{+\infty}\frac{1}{n!\times n}\left(1-\frac{x_3^n}{h_{\max}^n}\right)\frac{d^nI_{k,l,m}(0)}{dX_3^n}\right] \\ &= -\beta\left[I_{k,l,m}(0)\ln\left(\frac{x_3}{h_{\max}}\right) + \sum_{n=1}^{+\infty}\frac{1}{n!\times n}\left(\frac{x_3}{h_{\max}}\right)^n\frac{d^nI_{k,l,m}(0)}{dX_3^n}\right] + A_{k,l,m}, \end{aligned} \tag{13}$$

with $A_{k,l,m}$ constant, and $\beta = n_0/(\ln(h_{\max}) - \ln(h_{\min}))$. This then leads to the scaling laws for velocity components in the logarithmic region, i.e., Eqs. (2)–(4). More details for the derivation can be also found in Ref. [5].

B. Scalings of velocity gradient moments by attached eddies

Here we introduce a rigorous mathematical derivation of all moments of velocity gradients from a statistical perspective by using the AEM. The gradient operator on a single attached eddy (5) leads to

$$\nabla \boldsymbol{u}_{\text{one eddy}} = \frac{1}{h}\boldsymbol{T}\left(\frac{\boldsymbol{x}-\boldsymbol{x}_e}{h}\right), \tag{14}$$

where $\boldsymbol{T} = \nabla \boldsymbol{Q}$ is the velocity gradient tensor. Accordingly, the velocity gradient generated by all attached eddies can be expressed as

$$\nabla \boldsymbol{u}_{\text{total}} = \sum_{k=1}^{n_0} \frac{1}{h_k}\boldsymbol{T}\left(\frac{\boldsymbol{x}-\boldsymbol{x}_k}{h_k}\right). \tag{15}$$

Similar to Eq. (9), we introduce a velocity gradient contribution function of attached eddies, defined as (without summation convention)

$$L_{\overline{\overline{n}}}(X_3) \overset{\text{def}}{=} \iint_{-\infty}^{+\infty} \prod_{i=1}^{3}\prod_{j=1}^{3}\left(\frac{T_{ij}(\boldsymbol{X})}{h}\right)^{n_{ij}} dX_1 dX_2, \tag{16}$$

where $\overline{\overline{n}}$ is a 3×3 tensor with n_{ij} an arbitrary non-negative integer number. By further defining (without summation convention)

$$J_{\overline{\overline{n}}}(X_3) = \iint_{-\infty}^{+\infty} \prod_{i=1}^{3}\prod_{j=1}^{3} T_{ij}^{n_{ij}}(\boldsymbol{X}) dX_1 dX_2, \tag{17}$$

Eq. (16) is written as

$$L_{\overline{\overline{n}}}(X_3) = \frac{1}{h^N} J_{\overline{\overline{n}}}(X_3), \tag{18}$$

where $N = \sum_{i=1}^{3}\sum_{j=1}^{3} n_{ij}$. Similar to Eq. (10), we then define the cumulants of velocity gradients as

$$\mu_{\overline{\overline{n}}}(x_3) \overset{\text{def}}{=} n_0 \int_{h_{\min}}^{h_{\max}} L_{\overline{\overline{n}}}(X_3) p(h) dh. \tag{19}$$

Substituting Eqs. (8) and (18) to (19), we obtain

$$\mu_{\overline{\overline{n}}}(x_3) = \beta \int_{h_{\min}}^{h_{\max}} \frac{J_{\overline{\overline{n}}}(X_3)}{h^{N+1}} dh. \tag{20}$$

Another basic assumption in the AEM is that an attached eddy does not contribute to the velocity field at a location beyond its height. This assumption is important in the derivation since it allows one to delineate the influence range of each attached eddy. Using the same assumption as Woodcock and Marusic [5], for velocity gradient tensor we obtain

$$T_{ij}(\boldsymbol{X}) = 0, \quad \text{for} \quad x_3 > h, \tag{21}$$

and Eq. (20) writes

$$\mu_{\overline{\overline{n}}}(x_3) = \begin{cases} \beta \int_{x_3}^{h_{\max}} \frac{J_{\overline{\overline{n}}}(X_3)}{h^{N+1}} dh, & \text{for} \quad x_3 > h_{\min}, \\ \beta \int_{h_{\min}}^{h_{\max}} \frac{J_{\overline{\overline{n}}}(X_3)}{h^{N+1}} dh, & \text{for} \quad x_3 \leqslant h_{\min}. \end{cases} \tag{22}$$

Considering the cases of logarithmic region, we can limit the calculations to $x_3 > h_{\min}$. Since $dh = -x_3/X_3^2 dX_3$, $1/h^{N+1} = (X_3/x_3)^{N+1}$, and the Taylor series of $J_{\overline{n}}(X_3)$ at $X_3 = 0$ is

$$J_{\overline{n}}(X_3) = \sum_{n=0}^{+\infty} \frac{d^n J_{\overline{n}}(0)}{dX_3^n} \frac{X_3^n}{n!}, \tag{23}$$

Eq. (22) becomes

$$\mu_{\overline{n}}(x_3) = \frac{\beta}{x_3^N} C_{\overline{n}}(x_3), \tag{24}$$

where $C_{\overline{n}}(x_3) = \sum_{n=0}^{+\infty} [d^n J_{\overline{n}}(0)/dX_3^n]/[n!(N+n)][1 - (x_3/h_{\max})^{N+n}]$. Focusing on the logarithmic region, following Ref. [5] we have $x_3/h_{\max} \ll 1$, therefore

$$C_{\overline{n}}(x_3) \approx \sum_{n=0}^{+\infty} \frac{d^n J_{\overline{n}}(0)/dX_3^n}{n!(N+n)}, \tag{25}$$

indicating that $C_{\overline{n}}(x_3)$ can be considered as constant.

Therefore, we can finally derive the scaling laws of velocity gradient moments as

$$\mu_{\overline{n}}(x_3) \propto \frac{1}{x_3^N}. \tag{26}$$

From the literature, the moments of longitudinal velocity gradients are usually important, since they are sometimes analogous to the cases of homogeneous isotropic turbulence. For example, Ref. [48] derived the interscale relations for the moments of longitudinal velocity gradients and increments in homogeneous isotropic turbulence, and directly applied the results to channel flows. References [47,49] further illustrated that the moments of longitudinal velocity gradients lead to similar normalized values, such as the skewness, among different directions in anisotropic flows. In the present paper, we then follow these works and focus on the longitudinal velocity gradients by using the AEM. According to Eq. (26), the second- and third-order moments of longitudinal velocity gradients should satisfy the following scalings:

$$\left\langle \left(\frac{\partial u_1}{\partial x_1}\right)^2 \right\rangle \propto \frac{1}{x_3^2}, \quad \left\langle \left(\frac{\partial u_2}{\partial x_2}\right)^2 \right\rangle \propto \frac{1}{x_3^2}, \quad \left\langle \left(\frac{\partial u_3}{\partial x_3}\right)^2 \right\rangle \propto \frac{1}{x_3^2}, \tag{27}$$

$$\left\langle \left(\frac{\partial u_1}{\partial x_1}\right)^3 \right\rangle \propto \frac{1}{x_3^3}, \quad \left\langle \left(\frac{\partial u_2}{\partial x_2}\right)^3 \right\rangle \propto \frac{1}{x_3^3}, \quad \left\langle \left(\frac{\partial u_3}{\partial x_3}\right)^3 \right\rangle \propto \frac{1}{x_3^3}. \tag{28}$$

Subsequently, the skewness S_1, S_2, and S_3 can be defined for the longitudinal streamwise, spanwise, and wall-normal velocity gradients respectively, i.e.,

$$S_1 = \frac{\left\langle \left(\frac{\partial u_1}{\partial x_1}\right)^3 \right\rangle}{\left\langle \left(\frac{\partial u_1}{\partial x_1}\right)^2 \right\rangle^{3/2}}, \quad S_2 = \frac{\left\langle \left(\frac{\partial u_2}{\partial x_2}\right)^3 \right\rangle}{\left\langle \left(\frac{\partial u_2}{\partial x_2}\right)^2 \right\rangle^{3/2}}, \quad S_3 = \frac{\left\langle \left(\frac{\partial u_3}{\partial x_3}\right)^3 \right\rangle}{\left\langle \left(\frac{\partial u_3}{\partial x_3}\right)^2 \right\rangle^{3/2}}. \tag{29}$$

Equations (27) and (28) indicate that S_1, S_2, and S_3 are all constants along wall direction x_3. This conclusion is in agreement with the applications in Refs. [47,48].

III. SCALINGS OF MOMENTS OF FIRST-ORDER VELOCITY DERIVATIVES

In this section, DNS datasets on turbulent channel flows at various Reynolds numbers ($\mathrm{Re}_\tau \approx$ 1000, 2000, and 5200, respectively) are employed to validate the scaling laws of velocity gradients. Here the friction Reynolds number is defined as $\mathrm{Re}_\tau = \mathrm{u}_\tau \delta/\nu$, where ν is fluid kinematic viscosity and $u_\tau = \sqrt{\tau_w/\rho}$ is the friction velocity with τ_w mean wall shear stress and ρ fluid density. The flow fields at $\mathrm{Re}_\tau \approx 1000$ and 5200 were produced by Lee and Moser [19] and accessed via the

Johns Hopkins Turbulence Database [50]. The DNS data at $\mathrm{Re}_\tau \approx 2000$ were produced by Hoyas and Jiménez [51].

A. Extraction of attached eddies

According to Townsend [3], the attached eddies are only a portion of the turbulent motions in wall turbulence, while the logarithmic terms in Eqs. (2) and (3) represent swirling motions on a large scale. Townsend claimed that these motions have no discernible effect on the energy transfer rate to smaller eddies through viscous dissipation. As a result, Townsend classified the swirling component as "inactive." This perspective underscores the complexity of boundary layer flows in wall turbulence, which encompasses various motion types, including attached eddies among others [52–54].

Our objective is to extract the velocity gradient field attributable specifically to attached eddies. We follow Hu *et al.* [23] and decompose the flow field into wall-attached eddies, wall-detached eddies, and small-scale Kolmogorov eddies by a simple spectral filtering. This decomposition scheme indicates that the attached eddies are in charge of the streamwise and spanwise velocity of the scale

$$\alpha_{1,2}^{\mathrm{AE}} x_3 < \lambda_{x_1} < \beta_{1,2}^{\mathrm{AE}} \delta, \quad x_3^+ > \gamma_{1,2}^{\mathrm{AE}}, \tag{30}$$

where α^{AE}, β^{AE}, and γ^{AE} are constants, the subscripts 1 and 2 denote the streamwise and spanwise velocity components, respectively, γ^{AE} denotes a viscous cutoff length, and λ_{x_1} is the streamwise wavelength. The superscript "+" indicates the viscous normalization by u_τ and ν. Moreover, the attached eddies are responsible for the wall-normal velocity of the scale

$$\alpha_3^{\mathrm{AE}} x_3 < \lambda_{x_1} < \beta_3^{\mathrm{AE}} x_3, \quad x_3^+ > \gamma_3^{\mathrm{AE}}, \tag{31}$$

where the subscript 3 denotes the wall-normal velocity component.

For channel flow, the constants in Eqs. (30) and (31) are set according to Ref. [23], i.e., $\alpha_1^{\mathrm{AE}} = 5.7$, $\alpha_{2,3}^{\mathrm{AE}} = 1$, $\beta_1^{\mathrm{AE}} = 4$, $\beta_2^{\mathrm{AE}} = 1$, $\beta_3^{\mathrm{AE}} = 5$, and $\gamma_{1,2,3}^{\mathrm{AE}} = 100$. Note that from Eqs. (30) and (31), attached eddies represent the medium-scale eddies; in contrast, wall-detached eddies are categorized as larger-scale eddies, primarily the scales where $\lambda_{x_1} \geqslant \beta_{1,2}^{\mathrm{AE}} \delta$ for (u_1, u_2) and $\lambda_{x_1} \geqslant \beta_3^{\mathrm{AE}} x_3$ for u_3. Additionally, the scales where $\lambda_{x_1} \leqslant \beta_{1,2}^{\mathrm{AE}} \delta$ for (u_1, u_2) and $\lambda_{x_1} \leqslant \beta_3^{\mathrm{AE}} x_3$ for u_3 represent small-scale Kolmogorov eddies.

We then define the logarithmic range to better compare the results. The details of this definition are slightly different in literature according to practical applications, while in the present contribution, the lower and upper bounds of the logarithmic range are determined by using the viscous cutoff [23] and boundary thickness [2,50,55,56] respectively. Specifically, the viscous cutoff is $x_3^+ = 100$ according to Eqs. (30) and (31), and the upper bound is defined as $x_3/\delta = 0.2$ [19,55]. As a consequence, the logarithmic ranges are $x_3^+ = 100$–200, 100–400, and 100–1040 for $\mathrm{Re}_\tau = 1000$, 2000, and 5200, respectively.

Under these definitions, the approximation of $x_3 \ll h_{\max}$ in the derivation of Eq. (25) can be verified. Taking the $\mathrm{Re}_\tau = 1000$ case as an example, $h_{\max}$ is half the height of the channel, corresponding to $x_3/h_{\max} \sim O(10^{-1})$ in the logarithmic range. Consequently, for the second-order moments of velocity gradient (i.e., $N = 2$) the relative error of Eq. (25) is on the order of 10^{-2}, while for the third-order moments the relative error is on the order of 10^{-3}.

B. Comparison between DNS results and AEM predictions

The second- and third-order moments of longitudinal velocity gradients of attached eddies in the logarithmic region, calculated from DNS data using Eqs. (30) and (31), are displayed in Fig. 2. It can be observed that the second- and third-order moments approximately follow x_3^{-2} and x_3^{-3}, respectively. These results are in agreement with the theoretical predictions in Eqs. (27) and (28). Here all third-order moments of longitudinal velocity gradients are negative. This can be explained

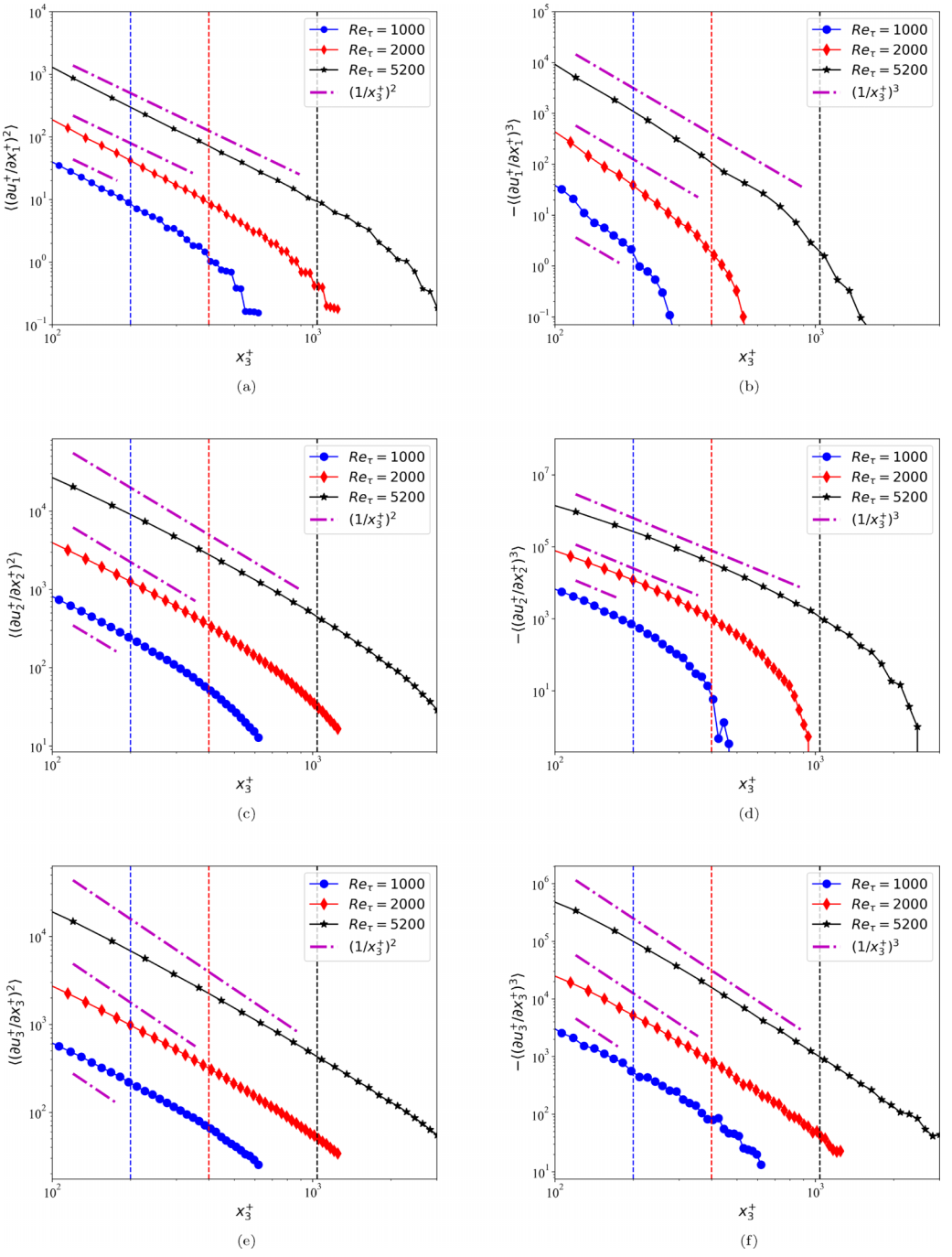

FIG. 2. Scalings of the second- and third-order moments of longitudinal (a), (b) streamwise, (c), (d) spanwise, and (e), (f) wall-normal velocity gradients of attached eddies, extracted by using Eqs. (30) and (31). The vertical dashed lines indicate the upper bounds of the logarithmic region at different Reynolds numbers.

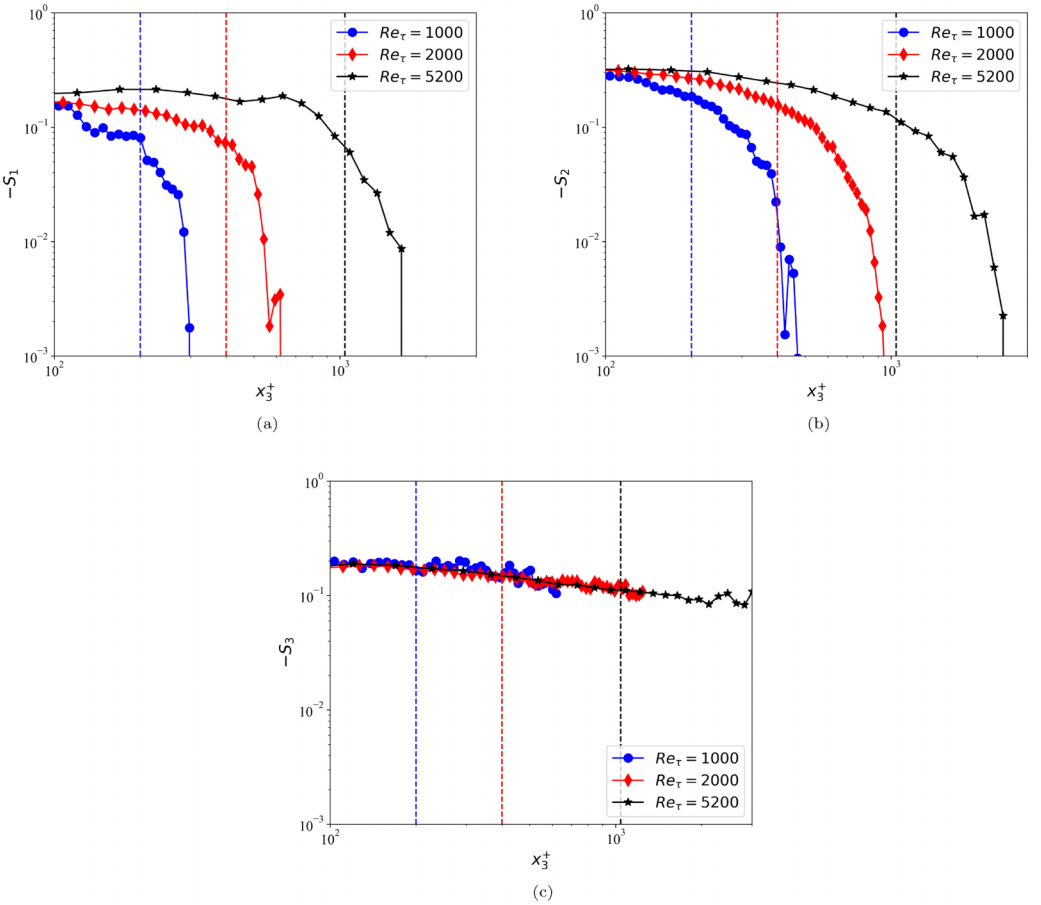

FIG. 3. Skewness of longitudinal (a) streamwise, (b) spanwise, and (c) wall-normal velocity gradients. The vertical dashed lines indicate the upper bounds of the logarithmic region at different Reynolds numbers.

by using traditional theories in isotropic turbulence [47,57], indicating that the energy transfers forward from large to small scales. The observation that the attached eddies generate negative values on the third-order moments, then implies that the energy can transfer from the attached eddies to smaller scales. This fact might inspire future investigations on considering the interscale energy transfer of attached eddies and improving the AEM.

In addition, it is found that the x_3^{-2} and x_3^{-3} laws are not always perfectly satisfied in Fig. 2. For example, in Figs. 2(c), 2(e), and 2(f) the slopes of DNS results are slightly less than theoretical predictions. These departures may stem from the method for extracting the attached eddies, which was introduced in the previous section. This method has been tested in the velocity field and shows good agreement with the AEM [23], while the present results might suggest more future reconsideration on the details.

In Fig. 3, we further calculate the skewness values of $-S_1$, $-S_2$, and $-S_3$, which are defined in Eq. (29) for the attached eddies. It is shown that the values of S_1, S_2, and S_3 are all negative and constant in the logarithmic region, indicating a forward energy transfer from large to small scales [58]. It can be observed that they are all of the order of 10^{-1} in the logarithmic regions, which is of the same magnitude as the canonical value in incompressible homogeneous isotropic turbulence [46,57,59]. For comparison, in compressible turbulence, this magnitude is usually much larger [60,61]. This fact might suggest that the interscale transfer of attached eddies is analogical to the

case of incompressible homogeneous isotropic turbulence. Related investigations, with comparison to the case of inhomogeneous free shear flows [47], are then expected to be performed in the future.

C. Scalings of velocity gradient moments of different types of eddies

It is now well recognized that the wall-attached eddies only describe a part of the turbulent fluctuations in wall-bounded flows. Specifically, they correspond to moderate scales, while the larger and smaller scales are wall-detached and Kolmogorov eddies, respectively [23]. The theoretical and numerical results in the previous sections are all on the attached eddies. Here we will also consider other types of eddies and calculate the velocity gradient moments respectively. We select the DNS data of turbulent channel flow at $\mathrm{Re}_\tau = 1000$ as an example. The attached eddies (AEs) are extracted by using Eqs. (30) and (31), resulting in larger-scale detached eddies (DEs) and small-scale Kolmogorov eddies (SEs). The moments of longitudinal velocity gradients of these different types of eddies are calculated respectively in Fig. 4. For comparison, the moments of all-scale longitudinal velocity gradients are also plotted (the "All" curves in Fig. 4).

In Fig. 4, the contributions of different types of eddies to the moments of velocity gradients are compared. In the logarithmic region (i.e., $x_3^+ = 100$–200), the DE part always contributes the least. This can be easily understood since the DE part corresponds to large-scale structures with a small magnitude of velocity gradients. We remark that differing from the moments of velocity [23], the AE part is no longer the dominant contribution to the moments of velocity gradients. Focusing on the logarithmic region: in Figs. 4(c)–4(f) the contribution of the AE part is approximately the same magnitude as the SE part; in Figs. 4(a) and 4(b), the SE part is the dominant contribution. These facts are also reasonable since the velocity gradients are small-scale quantities. Therefore, the velocity gradient statistics contain significant contributions from small-scale eddies. However, it indicates that second- and third-order moments of velocity gradients, or physically, the dissipation rate and energy transfer, respectively, are not dominated by attached eddies but by small-scale eddies.

Interestingly, SE dominates velocity gradients in the streamwise direction [Figs. 4(a) and 4(b)] while not in wall-normal and spanwise directions [Figs. 4(c)–4(f)]. This fact might indicate that the small-scale structures in the streamwise direction are very close to homogeneous isotropic turbulence without being affected by mean shear. It then explains and supports Ref. [48], where the dynamics of velocity gradient skewness is derived in homogeneous isotropic turbulence but can be used analogically to the streamwise velocity component. Another interesting observation is that in all subfigures of Fig. 4, the moments of full-scale longitudinal velocity gradients (i.e., the "All" curves) satisfy new scalings in the logarithmic region: all second-order moments satisfy an x_3^{-1} scaling, while all third-order moments satisfy an $x_3^{-1.5}$ scaling. Clearly, these scalings are not predicted by using the theories of attached eddies in Sec. II, implying the limitation of AEM in describing the wall-normal scalings of the moments of velocity gradients.

IV. SCALINGS OF MOMENTS OF HIGHER-ORDER VELOCITY DERIVATIVES

Considering the attached eddies, it is also possible to expand the theoretical derivations to higher-order velocity derivatives. For example, according to Eq. (14), we can derive the velocity Hessian of an attached eddy as a third-order tensor:

$$\frac{\partial^2 u_i}{\partial x_j \partial x_k} = \frac{1}{h^2}\frac{\partial^2 Q_i}{\partial X_j \partial X_k}, \tag{32}$$

and an nth-order partial derivative of velocity is a $(n+1)$th-order tensor ($n \geqslant 3$), as

$$\frac{\partial^n u_i}{\partial x_{j_1}\partial x_{j_2}\cdots\partial x_{j_n}} = \frac{1}{h^n}\frac{\partial^n Q_i}{\partial X_{j_1}\partial X_{j_2}\cdots\partial X_{j_n}}, \tag{33}$$

with $i, j, k, j_1, j_2, \ldots, j_n \in (1, 2, 3)$.

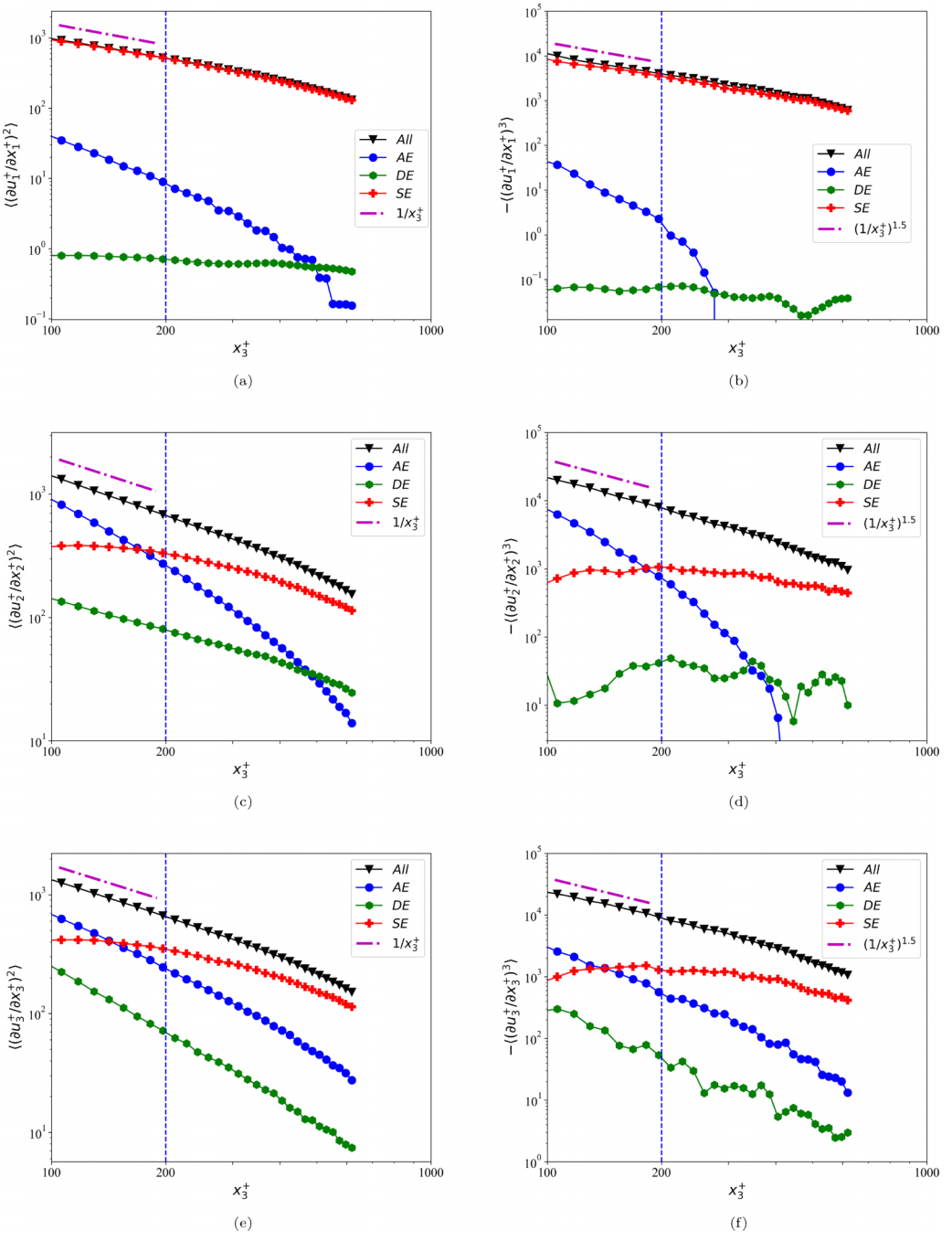

FIG. 4. Scalings of second- and third-order moments of longitudinal (a), (b) streamwise, (c), (d) spanwise, and (e), (f) wall-normal velocity gradients from all eddies (All), the attached eddies (AEs), the detached eddies (DEs), and small-scale eddies (SEs). The vertical dashed lines indicate the upper bound of the logarithmic region at $\mathrm{Re}_\tau = 1000$.

To simplify the derivation of arbitrary moments of velocity Hessian, here we focus on 3 components of the total 27 velocity Hessian components:

$$\frac{\partial^2 u_1}{\partial x_1^2} = \frac{1}{h^2}\frac{\partial^2 Q_1}{\partial X_1^2}, \quad \frac{\partial^2 u_2}{\partial x_2^2} = \frac{1}{h^2}\frac{\partial^2 Q_2}{\partial X_2^2}, \quad \frac{\partial^2 u_3}{\partial x_3^2} = \frac{1}{h^2}\frac{\partial^2 Q_3}{\partial X_3^2}. \tag{34}$$

Similar to Eq. (21), we have assumptions

$$\frac{\partial^2 Q_1}{\partial X_1^2} \approx 0, \quad \frac{\partial^2 Q_2}{\partial X_2^2} \approx 0, \quad \frac{\partial^2 Q_3}{\partial X_3^2} \approx 0, \quad \text{for} \quad x_3 > h, \tag{35}$$

and can define the velocity Hessian contribution function of attached eddies as

$$\begin{aligned} L_{k,l,m}(X_3) &\overset{\text{def}}{=} \frac{1}{h^{2k+2l+2m}} \iint_{-\infty}^{+\infty} \left(\frac{\partial^2 Q_1}{\partial X_1^2}\right)^k \left(\frac{\partial^2 Q_2}{\partial X_2^2}\right)^l \left(\frac{\partial^2 Q_3}{\partial X_3^2}\right)^m dX_1 dX_2 \\ &= \frac{1}{h^{2k+2l+2m}} J_{k,l,m}(X_3). \end{aligned} \tag{36}$$

Additionally, we can define the cumulants of velocity Hessian as

$$\begin{aligned} \mu_{k,l,m}(x_3) &\overset{\text{def}}{=} n_0 \int_{h_{\min}}^{h_{\max}} L_{k,l,m}(X_3) p(h) dh \\ &= \beta \int_{h_{\min}}^{h_{\max}} \frac{1}{h^{2k+2l+2m+1}} J_{k,l,m}(X_3) dh. \end{aligned} \tag{37}$$

After a similar derivation as in Sec. II, we obtain

$$\mu_{k,l,m}(x_3) \propto \frac{1}{x_3^{2k+2l+2m}}. \tag{38}$$

Specifically, we write

$$\left\langle \left(\frac{\partial^2 u_1}{\partial x_1^2}\right)^2 \right\rangle \propto \frac{1}{x_3^4}, \quad \left\langle \left(\frac{\partial^2 u_2}{\partial x_2^2}\right)^2 \right\rangle \propto \frac{1}{x_3^4}, \quad \left\langle \left(\frac{\partial^2 u_3}{\partial x_3^2}\right)^2 \right\rangle \propto \frac{1}{x_3^4}, \tag{39}$$

$$\left\langle \left(\frac{\partial^2 u_1}{\partial x_1^2}\right)^3 \right\rangle \propto \frac{1}{x_3^6}, \quad \left\langle \left(\frac{\partial^2 u_2}{\partial x_2^2}\right)^3 \right\rangle \propto \frac{1}{x_3^6}, \quad \left\langle \left(\frac{\partial^2 u_3}{\partial x_3^2}\right)^3 \right\rangle \propto \frac{1}{x_3^6}. \tag{40}$$

For the moments of nth-order partial derivatives of velocity ($n \geqslant 3$), we also assume

$$\frac{\partial^n Q_1}{\partial X_1^n} \approx 0, \quad \frac{\partial^n Q_2}{\partial X_2^n} \approx 0, \quad \frac{\partial^n Q_3}{\partial X_3^n} \approx 0, \quad \text{for} \quad x_3 > h. \tag{41}$$

Analogously, we can obtain the following scaling law:

$$\mu_{k,l,m,n}(x_3) \propto \frac{1}{x_3^{n(k+l+m)}}. \tag{42}$$

Specifically, we write

$$\left\langle \left(\frac{\partial^n u_1}{\partial x_1^n}\right)^2 \right\rangle \propto \frac{1}{x_1^{2n}}, \quad \left\langle \left(\frac{\partial^n u_2}{\partial x_2^n}\right)^2 \right\rangle \propto \frac{1}{x_2^{2n}}, \quad \left\langle \left(\frac{\partial^n u_3}{\partial x_3^n}\right)^2 \right\rangle \propto \frac{1}{x_3^{2n}}, \tag{43}$$

$$\left\langle \left(\frac{\partial^n u_1}{\partial x_1^n}\right)^3 \right\rangle \propto \frac{1}{x_3^{3n}}, \quad \left\langle \left(\frac{\partial^n u_2}{\partial x_2^n}\right)^3 \right\rangle \propto \frac{1}{x_3^{3n}}, \quad \left\langle \left(\frac{\partial^n u_3}{\partial x_3^n}\right)^3 \right\rangle \propto \frac{1}{x_3^{3n}}. \tag{44}$$

We use the DNS data of turbulent channel flows at $\mathrm{Re}_\tau = 1000$, 2000, and 5200 for validation. The part of attached eddies is extracted by using Eqs. (30) and (31). The second- and third-order

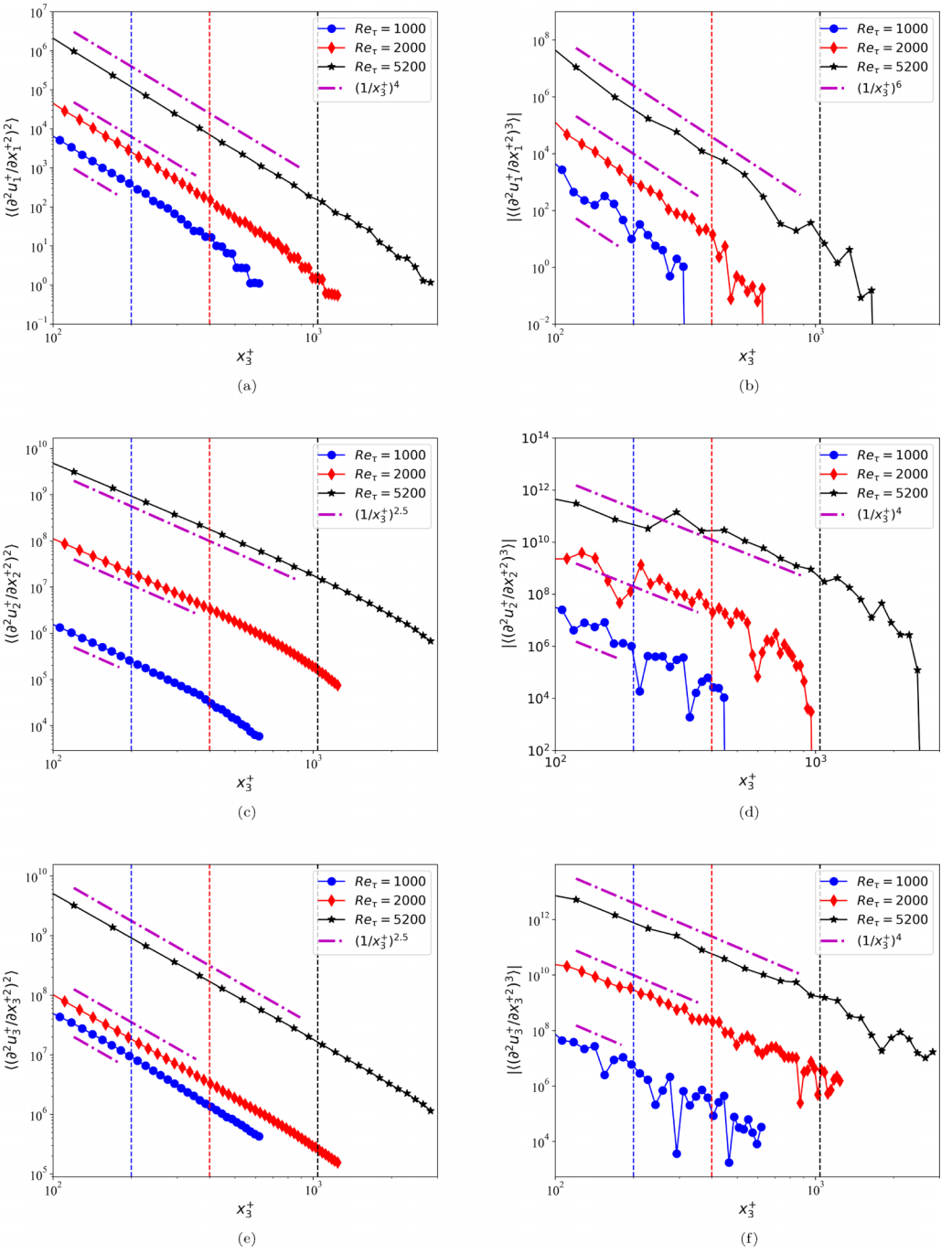

FIG. 5. Scalings of the second- and third-order moments of the three velocity Hessian components: (a), (b) $\partial^2 u_1/\partial x_1^2$, (c), (d) $\partial^2 u_2/\partial x_2^2$, and (e), (f) $\partial^2 u_3/\partial x_3^2$ of the attached eddies, extracted by using Eqs. (30) and (31). The vertical dashed lines indicate the upper bounds of the logarithmic region at different Reynolds numbers.

moments of the three velocity Hessian components described in Eqs. (39) and (40) are then calculated on the extracted fields. It can be observed that the predicted scalings (-4 and -6 for second- and third-order moments, respectively) are only well satisfied in the streamwise direction, i.e., Figs. 5(a) and 5(b). In the other directions, the scalings show departures from predictions. This fact is perhaps also understandable since the present extraction method uses Fourier filters, but perhaps it is too crude to consider attached eddies as a summation of some pure Fourier modes. Therefore, these facts might call for future improvement of the methods for extracting the attached eddies. Another possibility is that the AEM is inherently an inviscid theory, while the velocity Hessian is sensitive to the viscous effect, thus the departure might be due to the incapability of the AEM for the viscous effect.

V. CONCLUSIONS

The AEM has been considered as an effective framework for describing the energy-containing part of the logarithmic region of wall-bounded turbulence. According to this model, the logarithmic laws of velocity and second-order moments of velocity fluctuations have been deduced and verified in the literature. However, the moments for velocity gradients, which correspond to interscale energy transfer and dissipation, are not visited yet. In this work, we derive the scaling laws of arbitrary moments of velocity gradients analytically by using the AEM. Specifically, the second- and third-order moments of velocity gradients of the attached eddies (corresponding to moderate-scale structures) should exhibit power laws with exponents of -2 and -3, respectively. The decomposition scheme proposed by Hu *et al.* [23] is then employed to extract the flow fields of attached eddies from the DNS data of turbulent channel flows at $\mathrm{Re}_\tau = 1000$, 2000, and 5200, showing good agreement. The results illustrate that the decomposition scheme of Hu *et al.* [23] correctly extracts the attached eddies. It also indicates that the AEM can correctly predict the scalings of interscale energy transfer of moderate-scale structures, implying the forward energy cascade among the multiscale attached eddies.

However, it is well known that velocity gradients are rather small-scale quantities. In fact, the wall scalings of second- and third-order moments of all-scale velocity gradients are approximately -1 and -1.5, respectively, which are interestingly half of the scaling exponent of attached eddies. This fact may be due to the non-negligible influence of small-scale Kolmogorov eddies, which contain little kinetic energy but contribute a great amount to the moments of velocity gradients and cannot be explained by the AEM. Therefore, we conclude that the AEM does not correctly describe the wall behavior of moments of velocity gradients in all-scale (nonfiltered) velocity gradient fields. Also, the -1 and -1.5 scalings call for the development of other models for explanation in the future.

In addition, we show that although the present extraction method of attached eddies yields agreement with AEM predictions for the moments of velocity gradients, there exist obvious discrepancies in the moments of spanwise and wall-normal velocity Hessian. This fact is perhaps also understandable since the present extraction method uses Fourier filters, but perhaps it is too crude to consider attached eddies as a summation of some Fourier modes. Future investigations are therefore expected to be performed to improve the extraction method of attached eddies. Another possibility is that the AEM is inherently an inviscid theory, while the velocity Hessian is sensitive to the viscous effect, thus the departure might be due to the incapability of the AEM for the viscous effect.

Finally, we would like to mention that attached eddies are turbulent motions in the outer region, thus the AEM cannot be directly used in the inner region, e.g., for near-wall modeling purposes in wall-modeled large-eddy simulations.

ACKNOWLEDGMENTS

We acknowledge the financial support from the National Natural Science Foundation of China (Grants No. 12388101, No. 12372214, No. 11972175, and No. U2341231), the Fundamental Research Funds for the Central Universities (lzujbky-2024-oy10), and the Science Center for Gas Turbine Project (Grant No. P2022-C-III-001-001).

[1] A. J. Smits, B. J. McKeon, and I. Marusic, High Reynolds number wall turbulence, Annu. Rev. Fluid Mech. **43**, 353 (2011).
[2] I. Marusic, J. P. Monty, M. Hultmark, and A. J. Smits, On the logarithmic region in wall turbulence, J. Fluid Mech. **716**, R3 (2013).
[3] A. A. Townsend, *The Structure of Turbulent Shear Flow* (Cambridge University Press, Cambridge, UK, 1976).
[4] A. E. Perry and M. S. Chong, On the mechanism of wall turbulence, J. Fluid Mech. **119**, 173 (1982).
[5] J. D. Woodcock and I. Marusic, The statistical behaviour of attached eddies, Phys. Fluids **27**, 015104 (2015).
[6] I. Marusic and J. P. Monty, Attached eddy model of wall turbulence, Annu. Rev. Fluid Mech. **51**, 49 (2019).
[7] X. I. A. Yang and C. Meneveau, Hierarchical random additive model for wall-bounded flows at high Reynolds numbers, Fluid Dyn. Res. **51**, 011405 (2019).
[8] R. Hu, D. Dong, and R. Vinuesa, General attached eddies: Scaling laws and cascade self-similarity, Phys. Rev. Fluids **8**, 044603 (2023).
[9] L. Wang, R. Hu, and X. Zheng, A scaling improved inner-outer decomposition of near-wall turbulent motions, Phys. Fluids **33**, 045120 (2021).
[10] C. Meneveau and I. Marusic, Generalized logarithmic law for high-order moments in turbulent boundary layers, J. Fluid Mech. **719**, R1 (2013).
[11] C. M. de Silva, I. Marusic, J. D. Woodcock, and C. Meneveau, Scaling of second-and higher-order structure functions in turbulent boundary layers, J. Fluid Mech. **769**, 654 (2015).
[12] X. I. A. Yang, I. Marusic, and C. Meneveau, Moment generating functions and scaling laws in the inertial layer of turbulent wall-bounded flows, J. Fluid Mech. **791**, R2 (2016).
[13] X. I. A. Yang, I. Marusic, and C. Meneveau, Hierarchical random additive process and logarithmic scaling of generalized high order, two-point correlations in turbulent boundary layer flow, Phys. Rev. Fluids **1**, 024402 (2016).
[14] X. I. A. Yang, R. Baidya, P. Johnson, I. Marusic, and C. Meneveau, Structure function tensor scaling in the logarithmic region derived from the attached eddy model of wall-bounded turbulent flows, Phys. Rev. Fluids **2**, 064602 (2017).
[15] J. H. Xie, C. de Silva, R. Baidya, X. I. A. Yang, and R. Hu, Third-order structure function in the logarithmic layer of boundary-layer turbulence, Phys. Rev. Fluids **6**, 074602 (2021).
[16] J. Jiménez and S. Hoyas, Turbulent fluctuations above the buffer layer of wall-bounded flows, J. Fluid Mech. **611**, 215 (2008).
[17] M. Hultmark, M. Vallikivi, S. C. C. Bailey, and A. J. Smits, Turbulent pipe flow at extreme Reynolds numbers, Phys. Rev. Lett. **108**, 094501 (2012).
[18] R. J. A. M. Stevens, M. Wilczek, and C. Meneveau, Large-eddy simulation study of the logarithmic law for second- and higher-order moments in turbulent wall-bounded flow, J. Fluid Mech. **757**, 888 (2014).
[19] M. K. Lee and R. D. Moser, Direct numerical simulation of turbulent channel flow up to $\mathrm{Re}_\tau \approx 5200$, J. Fluid Mech. **774**, 395 (2015).
[20] Y. Yamamoto and Y. Tsuji, Numerical evidence of logarithmic regions in channel flow at $\mathrm{Re}_\tau = 8000$, Phys. Rev. Fluids **3**, 012602(R) (2018).
[21] A. Mehrez, J. Philip, Y. Yamamoto, and Y. Tsuji, Pressure and spanwise velocity fluctuations in turbulent channel flows: Logarithmic behavior of moments and coherent structures, Phys. Rev. Fluids **4**, 044601 (2019).
[22] W. J. Baars and I. Marusic, Data-driven decomposition of the streamwise turbulence kinetic energy in boundary layers. Part 2. Integrated energy and A_1, J. Fluid Mech. **882**, A26 (2020).
[23] R. Hu, X. I. A. Yang, and X. Zheng, Wall-attached and wall-detached eddies in wall-bounded turbulent flows, J. Fluid Mech. **885**, A30 (2020).
[24] R. Deshpande, J. P. Monty, and I. Marusic, Active and inactive components of the streamwise velocity in wall-bounded turbulence, J. Fluid Mech. **914**, A5 (2021).
[25] S. Pirozzoli, J. Romero, M. Fatica, R. Verzicco, and P. Orlandi, One-point statistics for turbulent pipe flow up to $\mathrm{Re}_\tau \approx 6000$, J. Fluid Mech. **926**, A28 (2021).

[26] L. Wang, C. Pan, J. Wang, and Q. Gao, Statistical signatures of component wall-attached eddies in proper orthogonal decomposition modes of a turbulent boundary layer, J. Fluid Mech. **944**, A26 (2022).
[27] M. Puccioni, M. Calaf, E. R. Pardyjak, S. Hoch, T. J. Morrison, A. Perelet, and G. V. Iungo, Identification of the energy contributions associated with wall-attached eddies and very-large-scale motions in the near-neutral atmospheric surface layer through wind LiDAR measurements, J. Fluid Mech. **955**, A39 (2023).
[28] J. Yao, S. Rezaeiravesh, P. Schlatter, and F. Hussain, Direct numerical simulation of turbulent pipe flow up to $\mathrm{Re}_\tau = 5200$, J. Fluid Mech. **956**, A18 (2023).
[29] A. Lozano-Durán, O. Flores, and J. Jiménez, The three-dimensional structure of momentum transfer in turbulent channels, J. Fluid Mech. **694**, 100 (2012).
[30] Y. Hwang, Statistical structure of self-sustaining attached eddies in turbulent channel flow, J. Fluid Mech. **767**, 254 (2015).
[31] J. Hwang and H. J. Sung, Wall-attached structures of velocity fluctuations in a turbulent boundary layer, J. Fluid Mech. **856**, 958 (2018).
[32] C. Cheng, W. Li, A. Lozano-Durán, and H. Liu, Identity of attached eddies in turbulent channel flows with bidimensional empirical mode decomposition, J. Fluid Mech. **870**, 1037 (2019).
[33] B. J. McKeon, Self-similar hierarchies and attached eddies, Phys. Rev. Fluids **4**, 082601(R) (2019).
[34] Q. Yang, A. P. Willis, and Y. Hwang, Exact coherent states of attached eddies in channel flow, J. Fluid Mech. **862**, 1029 (2019).
[35] R. Hu, X. Zheng, and S. Dong, Extracting discrete hierarchies of Townsend's wall-attached eddies, Phys. Fluids **34**, 061701 (2022).
[36] G. Wu, L. Fang, and J. Zhang, Numerical investigation and parametric analysis of an attached eddy model applied to inlet condition, Phys. Fluids **34**, 115143 (2022).
[37] J. Jiménez, Cascades in wall-bounded turbulence, Annu. Rev. Fluid Mech. **44**, 27 (2012).
[38] X. I. A. Yang and A. Lozano-Duran, A multifractal model for the momentum transfer process in wall-bounded flows, J. Fluid Mech. **824**, R2 (2017).
[39] Y. Mizuno, Spectra of energy transport in turbulent channel flows for moderate Reynolds numbers, J. Fluid Mech. **805**, 171 (2016).
[40] M. Cho, Y. Hwang, and H. Choi, Scale interactions and spectral energy transfer in turbulent channel flow, J. Fluid Mech. **854**, 474 (2018).
[41] M. Lee and R. D. Moser, Spectral analysis of the budget equation in turbulent channel flows at high Reynolds number, J. Fluid Mech. **860**, 886 (2019).
[42] W. Wang, C. Pan, and J. Wang, Energy transfer structures associated with large-scale motions in a turbulent boundary layer, J. Fluid Mech. **906**, A14 (2021).
[43] H. Wang, Z. Yang, T. Wu, and S. Wang, Coherent structures associated with interscale energy transfer in turbulent channel flows, Phys. Rev. Fluids **6**, 104601 (2021).
[44] T. R. Gungor, Y. Maciel, and A. G. Gungor, Energy transfer mechanisms in adverse pressure gradient turbulent boundary layers: Production and inter-component redistribution, J. Fluid Mech. **948**, A5 (2022).
[45] G. K. Batchelor, *The Theory of Homogeneous Turbulence* (Cambridge University Press, Cambridge, UK, 1953).
[46] W. J. T. Bos, L. Chevillard, J. F. Scott, and R. Rubinstein, Reynolds number effect on the velocity increment skewness in isotropic turbulence, Phys. Fluids **24**, 015108 (2012).
[47] H. K. Zhao, Y. W. Liu, L. Shao, L. Fang, and M. Dong, Existence of positive skewness of velocity gradient in early transition, Phys. Rev. Fluids **6**, 104608 (2021).
[48] G. X. Cui, H. B. Zhou, Z. S. Zhang, and L. Shao, A new dynamic subgrid eddy viscosity model with application to turbulent channel flow, Phys. Fluids **16**, 2835 (2004).
[49] X. Shao, J. Fang, and L. Fang, Non-equilibrium dissipation laws in a minimal two-scale wake model, Phys. Fluids **35**, 085105 (2023).
[50] J. Graham, K. Kanov, X. I. A. Yang, M. Lee, N. Malaya, C. C. Lalescu, R. Burns, G. Eyink, A. Szalay, R. D. Moser, and C. Meneveau, A web services accessible database of turbulent channel flow and its use for testing a new integral wall model for LES, J. Turbul. **17**, 181 (2016).
[51] S. Hoyas and J. Jiménez, Scaling of the velocity fluctuations in turbulent channels up to $\mathrm{Re}_\tau = 2003$, Phys. Fluids **18**, 011702 (2006).

[52] A. E. Perry and I. Marusic, A wall-wake model for the turbulence structure of boundary layers. Part 1. Extension of the attached eddy hypothesis, J. Fluid Mech. **298**, 361 (1995).
[53] I. Marušić and A. E. Perry, A wall-wake model for the turbulence structure of boundary layers. Part 2. Further experimental support, J. Fluid Mech. **298**, 389 (1995).
[54] W. J. Baars and I. Marusic, Data-driven decomposition of the streamwise turbulence kinetic energy in boundary layers. Part 1. Energy spectra, J. Fluid Mech. **882**, A25 (2020).
[55] J. Jiménez and R. D. Moser, What are we learning from simulating wall turbulence? Philos. Trans. R. Soc. A **365**, 715 (2007).
[56] J. Klewicki, P. Fife, and T. Wei, On the logarithmic mean profile, J. Fluid Mech. **638**, 73 (2009).
[57] M. Lesieur, *Turbulence in Fluids* (Kluwer Academic, Dordrecht, 1997).
[58] S. L. Tang and R. A. Antonia, Similarity for dissipation-scaled wall turbulence, J. Fluid Mech. **960**, A18 (2023).
[59] C. W. Van Atta and R. A. Antonia, Reynolds number dependence of skewness and flatness factors of turbulent velocity derivatives, Phys. Fluids **23**, 252 (1980).
[60] P. F. Yang, J. Fang, L. Fang, A. Pumir, and H. T. Xu, Low-order moments of the velocity gradient in homogeneous compressible turbulence, J. Fluid Mech. **947**, R1 (2022).
[61] C. S. Luo, P. F. Yang, and L. Fang, Low-order moments of velocity gradient tensors in two-dimensional isotropic turbulence, Symmetry **16**, 175 (2022).